Chemical Geology 633 (2023) 121569

Contents lists available at ScienceDirect

Chemical Geology

journal homepage: www.elsevier.com/locate/chemgeo

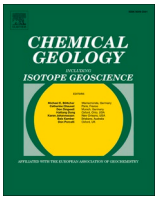

Low-$\delta^{18}O$ and negative-$\Delta^{199}Hg$ felsic igneous rocks in NE China: Implications for Early Cretaceous orogenic thinning

Changzhou Deng [a,b], Anzong Fu [c,d], Hongyan Geng [b,*], Deyou Sun [d,*], Guochun Zhao [e], Guangzhou Mao [b], Frédéric Moynier [f], Bernd Lehmann [g], Runsheng Yin [a]

[a] State Key Laboratory of Ore Deposit Geochemistry, Institute of Geochemistry, Chinese Academy of Sciences, Guiyang 550081, China
[b] Science Unit, Lingnan University, Hong Kong, China
[c] Heilongjiang Institute of Natural Resources Survey, Harbin 150036, China
[d] College of Earth Sciences, Jilin University, Changchun 130061, China
[e] Department of Earth Sciences, The University of Hong Kong, Pokfulam Road, Hong Kong, China
[f] Université de Paris, Institut de Physique du Globe de Paris, CNRS, 1 rue Jussieu, Paris 75005, France
[g] Mineral Resources, Technical University of Clausthal, Clausthal-Zellerfeld 38678, Germany

ARTICLE INFO

Editor: S Aulbach

Keywords:
Low-$\delta^{18}O$
Negative-$\Delta^{199}Hg$
Orogenic thinning
Magmatism
East China

ABSTRACT

Magmatic rocks carry key information to understand the processes of material cycling in the Earth's interior and record crucial clues to reconstruct the important tectonic evolution of the Earth. Therefore, it is of great importance to constrain the magma source (such as origin from crust or mantle, oceanic crust or continental crust, lower or upper continental crust) accurately, which however remains to be unraveled because of the variety magmatic sources and complex magmatic processes. High-precision stable isotopic analyses provide new tools to decipher the genesis of igneous rocks and to reconstruct their associated tectonic settings. Here, we report a pioneering work using integrated O-Hg-Hf-Nd isotopes to understand the genesis of the Early Cretaceous A-type granites and rhyolites from the Paleozoic-Mesozoic accretionary orogen in NE China. Low $\delta^{18}O$ zircon values (3.2–5.7‰) of the A-type rocks reveal a magma source affected by meteoric fluids. Their whole-rock negative $\Delta^{199}Hg$ values (−0.24 to −0.01‰), which are similar with the terrestrial systems but clearly different from the marine systems, indicate that hydrothermal alteration took place in the continental setting. Positive zircon $\varepsilon_{Hf}(t)$ (4.2–10.7) and mainly positive whole-rock $\varepsilon_{Nd}(t)$ (−0.5 to 2.4, mean = 1.2 ± 1.0, 1SD) values indicate that the magma source was dominated by juvenile crustal materials. This study suggests an elevated geothermal gradient due to the lithospheric thinning triggered by rollback and foundering of a Paleo-oceanic slab. The specific thermal anomaly caused the remelting of the altered upper continental crust, resulting in the formation of the A-type granites and rhyolites, with the characters of low-$\delta^{18}O$ and negative-$\Delta^{199}Hg$ values. Our study shows that Hg isotope, coupled with O and Nd—Hf isotopes, is a promising tool for petrogenetic studies.

1. Introduction

The late Mesozoic tectonic evolution in eastern China was characterized by the westward subduction of the Paleo-Pacific Plate, continental lithospheric thinning and associated large-scale magmatism (Griffin et al., 1998; Wu et al., 2005; Zhu and Zhu and Xu, 2019; Zhu and Sun, 2021). Significant Early Cretaceous lithospheric thinning in eastern China provides an important window in understanding craton modification, orogenic accretion and evolution, and mantle-crustal interaction (Zhu et al., 2012; Wu et al., 2019; Zheng et al., 2019; Liu et al., 2021; Yang et al., 2021). Although the Early Cretaceous A-type granites and rhyolites in NE China indicate an overall extensional setting (e.g., Wei et al., 2002a; Wang et al., 2013; Gong et al., 2018), their magma sources remain controversial. It is still unclear whether their magmas are sourced from partial melting of oceanic crust, lower continental crust, or upper continental crust. This controversy hinders the reconstruction of the Early Cretaceous tectonic settings in NE China. Moreover, the coeval occurrence of different Early Cretaceous igneous rocks, such as arc-like (Xu et al., 2013; Deng et al., 2019), within plate A-type (Jahn et al., 2001; Wang et al., 2013; Qin et al., 2019) and high Sr/Y adakitic rocks

* Corresponding authors.
E-mail addresses: helengeng@ln.edu.hk (H. Geng), sundy@jlu.edu.cn (D. Sun).

https://doi.org/10.1016/j.chemgeo.2023.121569
Received 7 March 2023; Received in revised form 22 May 2023; Accepted 23 May 2023
Available online 26 May 2023

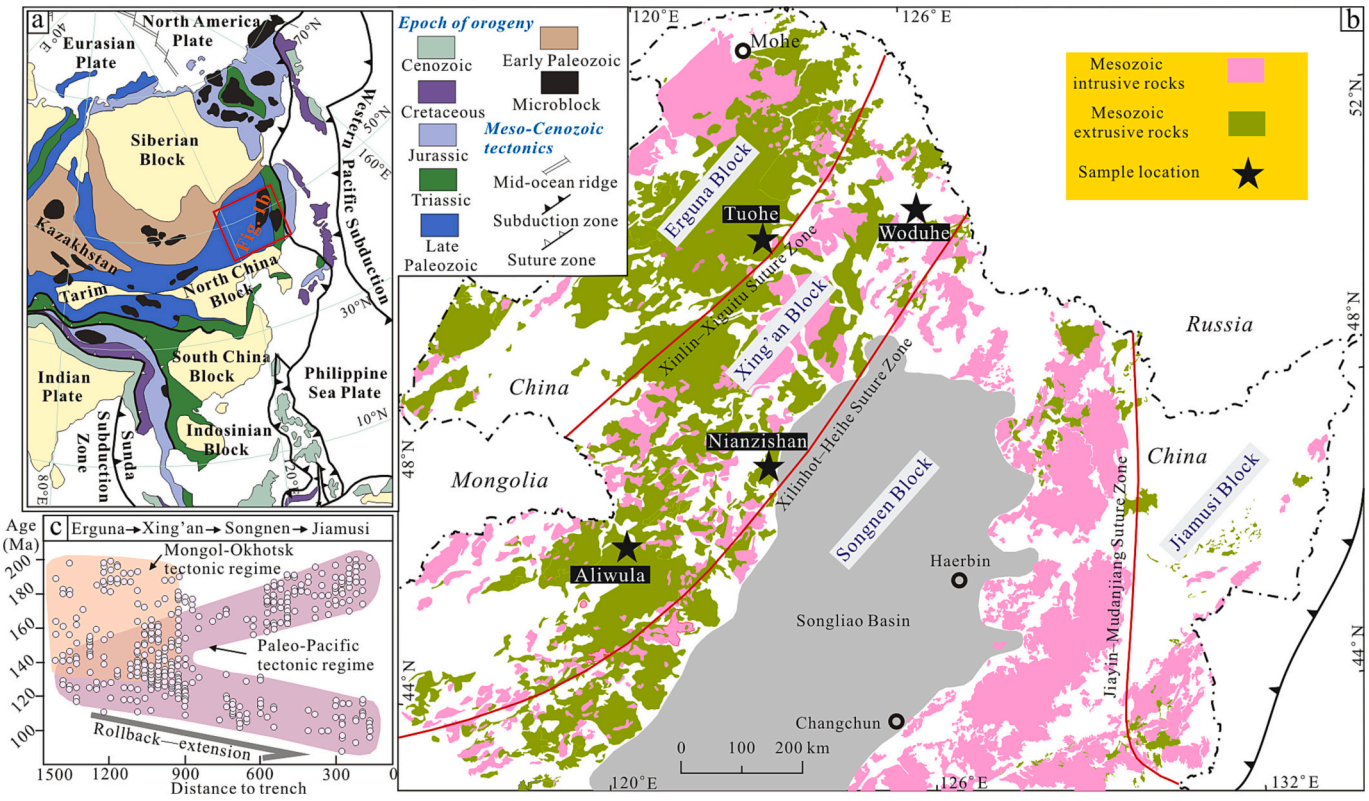

Fig. 1. (a) Simplified tectonic map of East Asia (modified after Safonova, 2017) showing the location of NE China. (b) Geological map of NE China (modified after Wu et al., 2011 and Xu et al., 2013) showing the distribution of the Mesozoic igneous rocks and location of samples in this study. (c) Ages and distances to the trench of Late Mesozoic igneous rocks in NE China, showing the temporal-spatial evolution of Mesozoic magmatism (Ji et al., 2019).

(Wang et al., 2019; Xu et al., 2020), makes it more complicated to understand the Early Cretaceous geodynamics and thermal-tectonic structure in NE China.

Igneous rocks have been used as a key tracer to decipher the geodynamic evolution of the earth, given that their geochemical characteristics ultimately reflect their source nature, and melt conditions (Rollinson, 1993). However, it is a great challenge to constrain the magma source accurately because of the varied magmatic sources and complex magmatic processes. Radio active isotopic systems (such as Sr-Nd-Hf) were traditionally used to distinguish the magma sourced from the depleted or enriched mantle (e.g., Salters and White, 1998). In particular, zircon oxygen isotope ratios (typically shown as $\delta^{18}O$) are regarded as the most reliable indicator of magma sources since it is resistant to subsolidus hydrothermal alteration or high-grade metamorphism (Valley et al., 1994; Page et al., 2007). Therefore, zircon $\delta^{18}O$ values are widely used to distinguish the post-magmatic hydrothermal alterations (Valley et al., 2005; Wei et al., 2008; Wang et al., 2017; Gevedon et al., 2021). Igneous rocks with low zircon $\delta^{18}O$ values (<5.5‰) indicate high temperature (800–1000 °C; Zheng, 1993) and the involvement of meteoric water (Valley et al., 2005; Bindeman et al., 2012; Boroughs et al., 2012; Smithies et al., 2015). However, O isotope composition itself is not capable to distinguish a meteoric water-altered upper continental crust from a seawater-altered oceanic crust, and additional isotopic systems are therefore required (e.g., Lackey et al., 2012).

Mercury is the only metal undergoing both large isotopic mass-dependent fractionation (MDF, defined as $\delta^{202}Hg$) and mass-independent fractionation (MIF, usually defined as $\Delta^{199}Hg$) (Bergquist and Blum, 2007). A variety of physical, chemical, or biological processes related to Hg biogeochemical cycling can trigger Hg-MDF (Smith et al., 2005; Blum et al., 2014), whereas only a few specific processes (e.g., Hg photochemical reactions) can trigger significant Hg-MIF (Bergquist and Blum, 2007; Blum et al., 2014). Combined with the MDF and MIF signatures, Hg isotope geochemistry has emerged as a reliable tracer to constrain the sources and processes of Hg in different geochemical processes (Blum et al., 2014; Yin et al., 2022). On Earth's surface, photochemical processes result in negative $\Delta^{199}Hg$ (−0.6 to 0‰) in terrestrial reservoirs (e.g., soil and vegetation) but positive $\Delta^{199}Hg$ (0 to 0.4‰) in oceanic reservoirs (e.g., seawater and marine sediments) (Blum et al., 2014). Notably, since Hg-MIF is resistant to magmatic and metamorphic processes (Moynier et al., 2021; Chen et al., 2022; Deng et al., 2022a; Yin et al., 2022), it is widely used to distinguish the marine sources from the terrestrial sources (Wang et al., 2021; Deng et al., 2022b; Tian et al., 2022).

This study examines Earth Cretaceous granite and rhyolite samples from NE China by investigating the whole-rock Hg isotopic compositions, zircon U–Pb–Hf–O isotopes and whole-rock Nd isotopes. Results show that these rocks were derived from the juvenile upper continental crust, indicating a thermal anomaly during the Early Cretaceous, which may be caused by the lithospheric thinning that occurred in the accretionary orogen in NE China.

2. Geological setting and samples

NE China is situated in the eastern part of the *E*-W-trending Central Asian Orogenic Belt (CAOB), one of the largest accretionary orogenic collages on Earth (Fig. 1a; Jahn, 2004; Xiao et al., 2015). It is characterized by a long history of accretion and collision of multiple microcontinents, terranes, and arc-back arc systems (Windley and Xiao, 2018). The microcontinents (Erguna, Xing'an, Songnen, and Jiamusi blocks from west to east; Fig. 1b) in NE China underwent a series of subduction processes, which include the subduction of the Paleo-Asian oceanic slab at Paleozoic-early Mesozoic, the southward subduction of the Mongol-Okhotsk Plate at late Paleozoic-late Jurassic (Yang et al.,

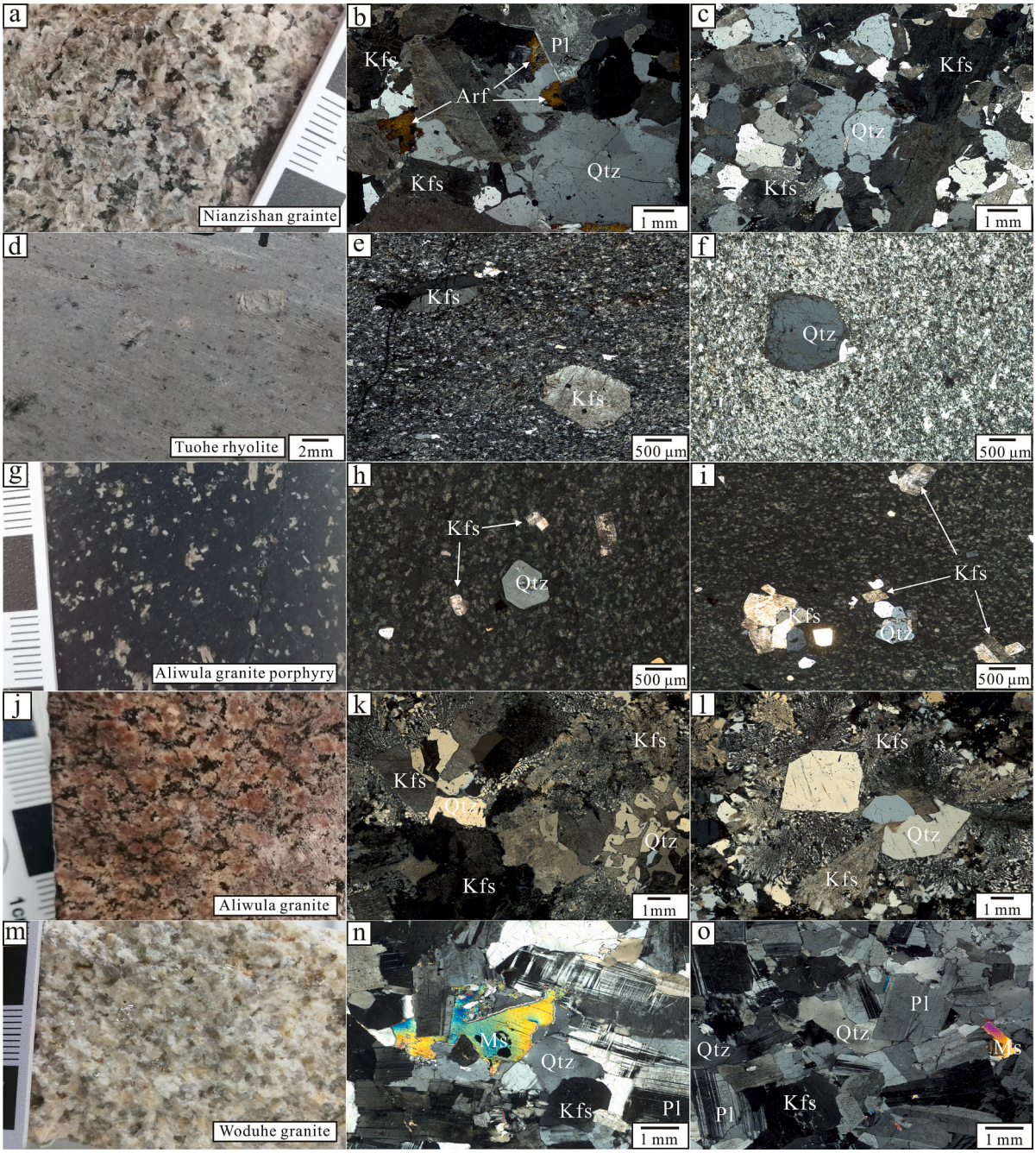

Fig. 2. Photographs and microphotographs showing the texture and mineralogy of the Nianzishan granite (a–c), Tuohe rhyolite (d–f), Aliwula granite porphyry (g–i), Aliwula granite (j–l) and Woduhe granite (m–o). Abbreviations: Pl, plagioclase; Q, quartz; Kfs, K-feldspar; Ms., muscovite; Arf, arfvedsonite.

2015; Deng et al., 2019), and the northwestward subduction of the Paleo-Pacific Plate at late Mesozoic (Wu et al., 2011; Xu et al., 2013). All continental blocks and fragments converged to the pre-Jurassic combined North and South China blocks following the final closure of the Paleo-Asian Ocean during the Late Permian-Middle Triassic (Cao et al., 2013; Wang et al., 2015; Eizenhöfer and Zhao, 2018; Zhao et al., 2018). The amalgamated eastern China continent then underwent northwestward subduction of the Paleo-Pacific oceanic slab during the late Mesozoic (Li et al., 2019), producing extensive magmatism (Fig. 1c; Ji et al., 2019; Ma and Xu, 2021).

This work studies the Early Cretaceous magmatic rocks distributed in the Erguna and Xing'an blocks (Fig. 1b) in NE China, including the Nianzishan granites, Tuohe rhyolites, Aliwula granite porphyry, Aliwula granites and Woduhe granites. The Nianzishan granites consist of K-feldspar (45 vol%), quartz (30 vol%), plagioclase (15 vol%), arfvedsonite (~7 vol%) (Figs. 2a-c) and aegirine (~1 vol%), with minor accessory minerals (~2 vol%) of zircon, magnetite and apatite. The Tuohe rhyolites consist of a fine-grained matrix (90 vol%) and medium- to fine-grained phenocrysts (5 vol%) of K-feldspar and quartz (Fig. 2d-f). The Aliwula granite porphyry consist of a fine-grained matrix (90 vol%) and phenocrysts (10 vol%) of quartz, K-feldspar (Fig. 2h-i) and minor riebeckite. The Aliwula granites show typical graphic texture and consist mainly of medium- to fine-grained quartz (35 vol%), K-feldspar (55 vol %) (Fig. 2j-l), plagioclase (5 vol%), riebeckite (~2 vol%), aegirine, and accessory minerals (zircon and magnetite). The Woduhe granites are composed of K-feldspar (20 vol%), plagioclase (35 vol%), quartz (35 vol %), muscovite (~8 vol%) (Fig. 2m-o), garnet (~1 vol%) and accessory minerals of zircon, apatite and opaque minerals.

Table 1
Total Hg contents and isotopic compositions of the Early Cretaceous granites and rhyolites in NE China.

Sample No.	Description	Hg contents (ppb)	δ^{199}Hg	δ^{200}Hg	δ^{201}Hg	δ^{202}Hg	Δ^{199}Hg	Δ^{200}Hg	Δ^{201}Hg
NZS-2	Granite	0.57	−0.13	−0.27	−0.44	−0.50	−0.01	−0.03	−0.07
NZS-4	Granite	0.93	−0.05	−0.06	0.08	0.23	−0.11	−0.18	−0.09
NZS-5	Granite	1.38	−0.22	−0.34	−0.60	−0.85	−0.01	0.09	0.04
NZS-12	Granite	0.25	−0.40	−0.49	−0.86	−0.98	−0.15	0.00	−0.13
NZS-13	Granite	0.65	−0.24	−0.20	−0.40	−0.31	−0.16	−0.04	−0.17
NZS-14	Granite	0.85	−0.11	0.01	−0.07	0.08	−0.12	−0.03	−0.13
NZS-15	Granite	1.15	−0.11	−0.02	−0.08	0.08	−0.13	−0.06	−0.14
TH-1	Rhyolite	0.43	−0.25	−0.06	−0.20	−0.03	−0.24	−0.04	−0.18
TH-2	Rhyolite	0.36	−0.22	−0.17	−0.39	−0.31	−0.14	−0.02	−0.16
TH-3	Rhyolite	0.85	−0.34	−0.27	−0.58	−0.47	−0.22	−0.03	−0.23
ALWY-1	Granite porphyry	0.53	−0.27	−0.32	−0.68	−0.83	−0.06	0.09	−0.05
ALWY-2	Granite porphyry	0.89	−0.29	−0.51	−0.63	−0.68	−0.11	−0.17	−0.12
ALWG-1	Granite	5.42	−0.51	−0.71	−1.11	−1.30	−0.18	−0.06	−0.13
ALWG-2	Granite	3.32	−0.32	−0.47	−0.72	−0.83	−0.11	−0.05	−0.10
ALWG-3	Granite	2.29	−0.30	−0.46	−0.73	−0.87	−0.08	−0.02	−0.08
WDH-1	Granite	0.16	−0.28	−0.33	−0.65	−0.73	−0.09	0.03	−0.11
WDH-3	Granite	0.30	−0.06	0.10	−0.00	0.18	−0.11	0.01	−0.14
WDH-4	Granite	0.15	−0.28	−0.23	−0.51	−0.44	−0.17	−0.01	−0.18
WDH-5	Granite	0.25	−0.44	−0.49	−0.76	−0.81	−0.23	−0.09	−0.15
WDH-7	Granite	0.16	−0.10	−0.02	−0.20	−0.09	−0.08	0.03	−0.13
WDH-8	Granite	0.66	−0.02	0.04	−0.11	−0.02	−0.01	0.05	−0.10
WDH-9	Granite	0.18	−0.27	−0.31	−0.56	−0.56	−0.13	−0.02	−0.14
WDH-13	Granite	0.18	−0.37	−0.34	−0.72	−0.74	−0.18	0.03	−0.16

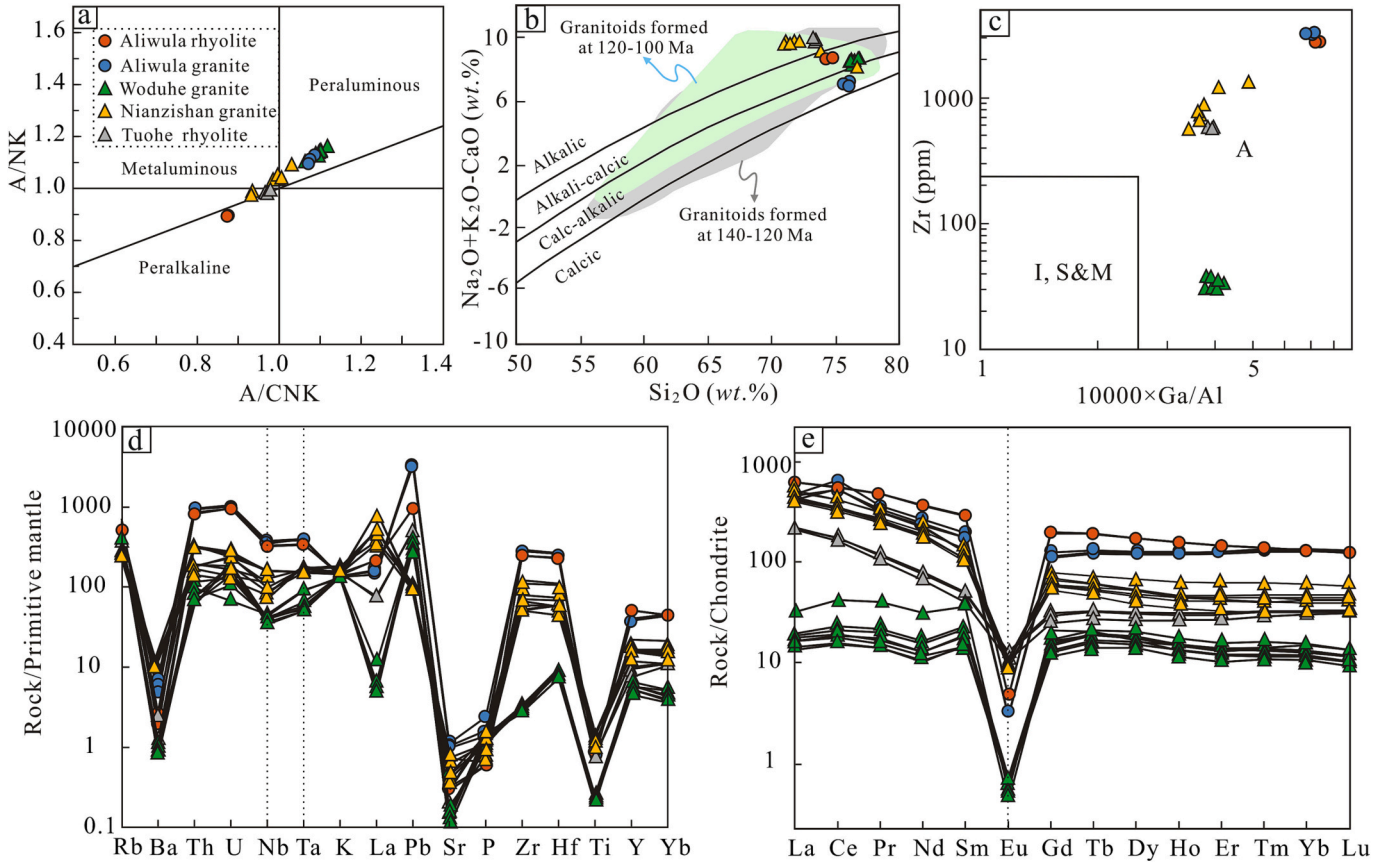

Fig. 3. (a) A/NK vs. A/CNK (after Maniar and Piccoli, 1989), (b) $Na_2O + K_2O$–CaO vs. SiO_2 (after Frost et al., 2001), the color areas are defined by Qin et al. (2019), and (c) Zr vs. 10,000 × Ga/Al plots (after Whalen et al., 1987). (d) Primitive mantle-normalized (Sun and McDonough, 1989) trace element spider grams and (e) Chondrite-normalized (Sun and McDonough, 1989) REE patterns for the A-type granites and rhyolites in NE China.

3. Methods

Whole-rock major and trace-element compositions, both conducted at the Institute of Geochemistry, Chinese Academy of Science (IGCAS), Guiyang, were analyzed by using X-ray fluorescence spectrometry and inductively coupled plasma mass spectrometry (ICP-MS), respectively. The fused glass disks were firstly prepared and then major element contents were analyzed. Trace element compositions were undertaken following the methods and procedures described by Gao et al. (2002). The analytical uncertainty for major and trace elements are better than

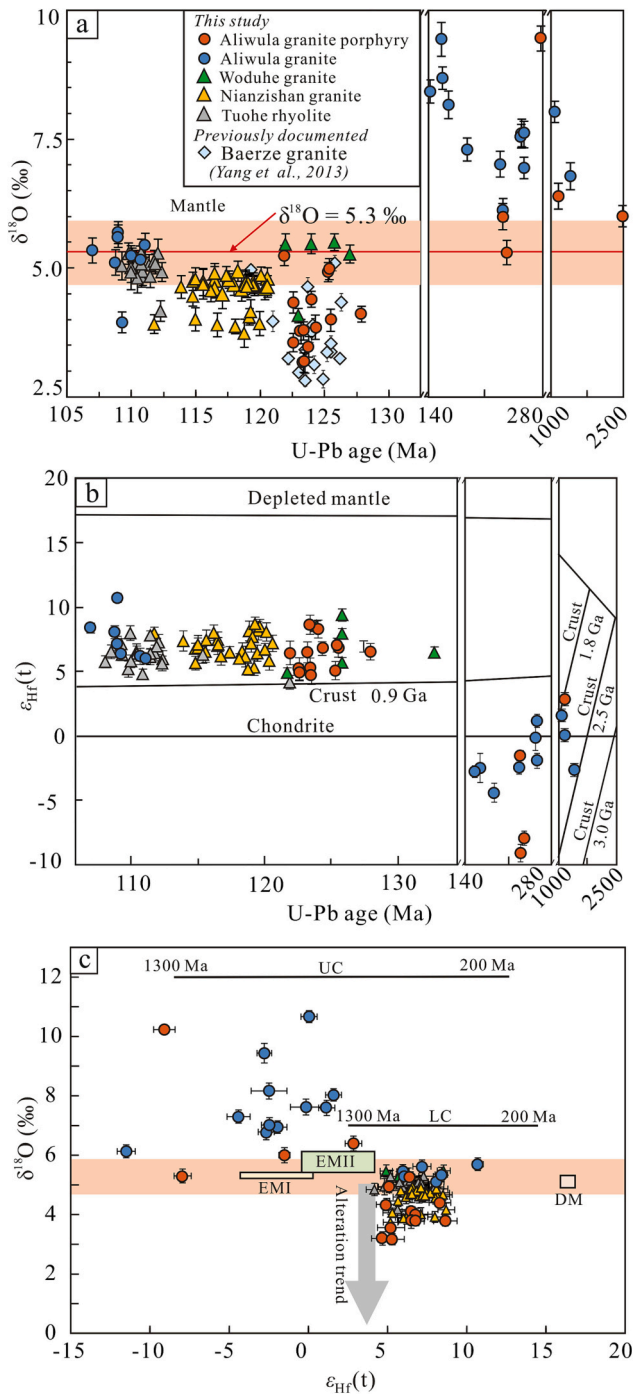

Fig. 4. (a) $\delta^{18}O$ values versus U—Pb ages of zircon grains. Data source for Baerze granite refers to Yang et al. (2013). (b) $\varepsilon_{Hf}(t)$ values versus U—Pb ages of zircon grains. (c) $\delta^{18}O$ vs. $\varepsilon_{Hf}(t)$ plots of the zircon grains, as well as different O—Hf isotope reservoirs. Oxygen isotopes for the upper crust (UC), EM1, EM2 and DM refer to Eiler (2001), for meteoric water to Drew et al. (2013); for the lower crust (LC) to Kempton and Harmon (1992). Hf isotopes for DM, EM1 and EM2 refer to Salters and White (1998).

1%, and 10%, respectively. The results are listed in Supplementary Table 1.

Six samples (TH-1, NZS-1, NZS-7, WDH-1, ALWY and ALWG) were processed for zircons separation according to the standard density and magnetic procedures, followed by hand-picking under a binocular microscope. The zircon grains then were mounted in epoxy resin together with zircon (91,500, Plešovice and Penglai). Zircon O isotopic analysis was performed using the Cameca IMS-1280 SIMS at the Guangzhou Institute of Geochemistry, Chinese Academy of Sciences. Oxygen isotopes were measured in multi-collector mode with two off-axis Faraday cups with each analysis consisting of 20 cycles × 4 s counting time. Oxygen isotopic results are reported with the conventional $\delta^{18}O$ notation in permil (‰) relative to Vienna Standard Mean Ocean Water (VSMOW). The instrumental mass fractionation (IMF) was corrected using in-house zircon standard Penglai with $\delta^{18}O$ value of 5.3 ± 0.1‰. Qinghu zircon, a zircon standard, was analyzed as an unknown to monitor the external precision, yielding a mean $\delta^{18}O$ of 5.7 ± 0.2‰ (n = 11). Detailed oxygen isotopic analytical procedure can refer to Li et al. (2010). The analytical results of studied rocks are listed in Supplementary Table 2.

Zircon U—Pb isotopic analysis was performed using laser ablation ICP–MS at the Wuhan Sample Solution Analytical Technology Co., Ltd., Wuhan, China. Detailed analytical procedures are available in Liu et al. (2010). Zircon GJ-1 was used as an external standard and ICPMSDataCal software was used to perform signals analysis, time-drift corrections and calibration. Concordia diagrams and weighted mean calculations were created using Isoplot/Ex_ver3 (Ludwig, 2003). The Plešovice zircon was treated as an unknown sample, and yielded a weighted mean $^{206}Pb/^{238}U$ age of 337.8 ± 0.87 Ma (2sd, n = 12), which is compatible with the recommended $^{206}Pb/^{238}U$ age of 337.13 ± 0.17 Ma (2sd) (Sláma et al., 2008). The results of U—Pb isotope dating of the zircons are listed in Supplementary Table 3.

In situ zircon Hf isotope analyses were performed at the Institute of Geochemistry, Chinese Academy of Sciences (IGCAS), using a Neptune Plus MC–ICP–MS equipped with a 193 nm laser. All zircon grains were analyzed in single-spot ablation mode with a spot size of 50 μm. Details of the analytical methods are provided by Wu et al. (2006). The weighted mean $^{176}Hf/^{177}Hf$ isotopic ratio of the GJ-1 zircon external standard was 0.282006 ± 0.000014 (2σ, n = 4), which is compatible with the recommended $^{176}Hf/^{177}Hf$ isotopic ratio of 0.282000 ± 0.000005 (2σ) (Morel et al., 2008). The zircon Lu—Hf isotopic data are presented in Supplementary Table 4.

Twenty-three fresh granite and rhyolite samples were collected from NE China for whole-rock Nd and Hg isotopic analyses. Prior to analyses, the samples were air-dried, crushed, powdered and sieved at 200 mesh. Whole-rock Hg and Nd isotope analyses were undertaken using a Neptune Plus multi-collector (MC) ICP–MS at IGCAS. The Nd isotope analyses were undertaken using a Neptune Plus multi-collector (MC) ICP–MS at (IGCAS), following the method by Wei et al. (2002b). Measured $^{143}Nd/^{144}Nd$ ratios were normalized to $^{146}Nd/^{144}Nd$ = 0.7219. The measured $^{143}Nd/^{144}Nd$ ratio of the GSB standard was 0.512440 ± 0.000008 (2σ, n = 4), which is within the uncertainty of the reported values (0.512439 ± 0.000010; Li et al., 2016). The whole-rock Nd isotopic compositions are presented in Supplementary Table 5.

Bulk Hg concentrations of the samples were measured using a DMA-80 Hg analyzer, with Hg detection limit of 0.01 ng/g. Measurements of standard sample (GSR-2, andesite) yielded Hg recoveries of 90–110%. Analysis of triplicate samples yielded uncertainty (2SD) of<10% for Hg. The samples were prepared for mercury isotope analysis following the double-stage thermal combustion and pre-concentration protocol (Zerkle et al., 2020). The double-stage thermal combustion system is composed of a quartz tube containing solid powder samples and two combustion furnaces (Huang et al., 2015). The combustion temperature of the first furnace is generally set as 950 °C for Hg release, meanwhile, the second furnace is set as 950–1000 °C for keeping constant temperature. The released Hg was captured by a 5 mL 40% (v/v, $3HNO_3$/1HCl) acid-trapping solution. The preconcentrated solutions were diluted to 0.5 ng/mL Hg and measured following Yin et al. (2016). Hg-MDF is expressed in $\delta^{202}Hg$ notation in units of ‰ referenced to the NIST-3133 Hg standard (analyzed before and after each sample):

$$\delta^{202}Hg(‰) = \left[\left(^{202}Hg/^{198}Hg_{sample}\right)/\left(^{202}Hg/^{198}Hg_{standard}\right) - 1\right] \times 1000$$

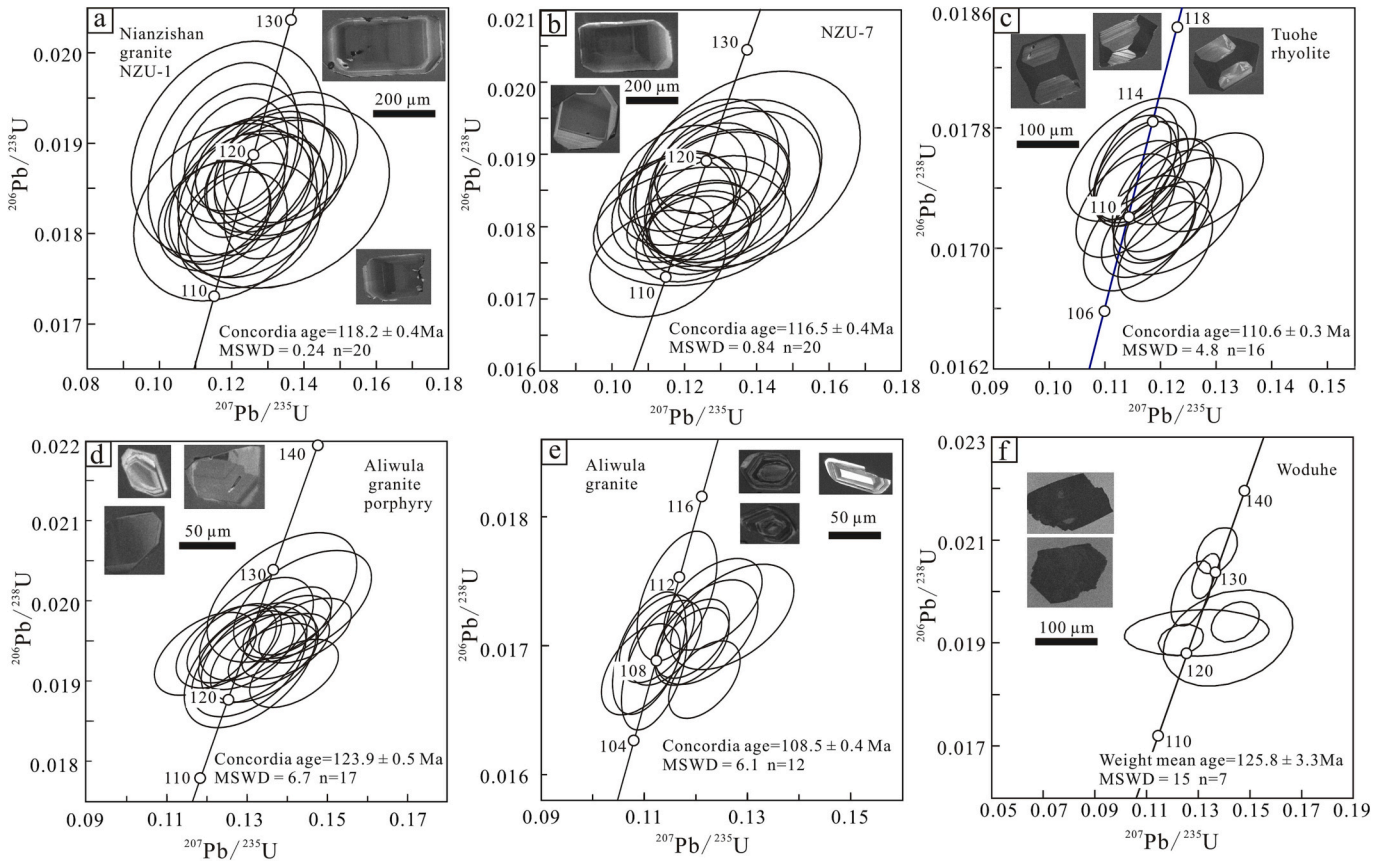

Fig. 5. Cathodoluminescence images of representative analyzed zircons and concordia or weighted zircon U—Pb age diagrams for the studied igneous rocks in NE China.

MIF is reported in Δ notation, which describes the difference between the measured $\delta^{xxx}Hg$ and the theoretically predicted $\delta^{xxx}Hg$ value, in units of ‰:

$$\Delta^{xxx}Hg = \delta^{xxx}Hg - \delta^{202}Hg \times \beta$$

β is 0.2520 for ^{199}Hg, 0.5024 for ^{200}Hg, and 0.7520 for ^{201}Hg (Blum and Bergquist, 2007). Analytical uncertainty was estimated based on the replication of the NIST-3177 standard solution. SRM GSR-2 (andesite) was prepared and measured in the same way as the samples. Result of GSR-2 ($\delta^{202}Hg$: −1.65 ± 0.10‰; $\Delta^{199}Hg$: −0.03 ± 0.06‰) agrees within uncertainty with those reported by Geng et al. (2018). The overall average and uncertainty of NIST-3177 ($\delta^{202}Hg$: −0.52 ± 0.10‰; $\Delta^{199}Hg$: −0.02 ± 0.06‰; $\Delta^{201}Hg$: 0.01 ± 0.08‰, 2SD, $n = 5$) agree well with previous studies (Blum and Berquist, 2007). The uncertainties of NIST-3177 with $\delta^{202}Hg$, $\Delta^{199}Hg$, and $\Delta^{201}Hg$ of 0.10‰, 0.06‰ and 0.08‰, respectively, represent the analytical uncertainties of our samples. Hg isotopic compositions of the samples are shown in Table 1.

4. Results

4.1. Whole-rock geochemistry

Samples in this study are felsic (SiO_2: 71.1–76.9 wt%), showing peralkaline to slightly metaluminous (Fig. 3a), alkalic to calc-alkalic geochemical features (Fig. 3b). Their high 10,000 × Ga/Al ratios (3.43–7.43) suggest an A-type granites affinity (Fig. 3c). Trace element compositions show that they are enriched in Rb, Th, U, Nb, Ta, Zr, Hf and heavy REEs, but depleted in Ba, Sr, P, Ti, and Eu (Figs. 3d-e).

4.2. Zircon O isotopic compositions

Zircon grains from the Nianzishan granite, Tuohe rhyolite and Woduhe granite show $\delta^{18}O$ values of 4.5 ± 0.3‰ (1SD, $n = 35$), 5.0 ± 0.3‰ (1SD, $n = 17$) and 5.2 ± 0.6‰, (1SD, n = 5), respectively. Magmatic zircon grains from the Aliwula granite porphyry and granite have low $\delta^{18}O$ values of 4.1 ± 0.7‰ (1SD, $n = 14$) and 5.2 ± 0.5‰ (1SD, $n = 8$), respectively, whereas xenocrysts/antecrysts have higher $\delta^{18}O$ values (5.3–10.2‰ for rhyolite and 6.1–10.7‰ for granite) (Fig. 4a).

4.3. Zircon U—Pb age

Zircon U—Pb isotopic data are presented in Fig. 5. Tuohe rhyolite (TH-1) and Nianzishan granite (NZS-1 and NZS-7) produce the concordant weighted mean $^{206}Pb/^{238}U$ ages of 110.8 ± 0.7 Ma, 118.3 ± 0.8 Ma and 116.5 ± 1.1 Ma (1σ), respectively. Because of the high U–Th–Pb contents, only seven concordant U—Pb ages were obtained for the Woduhe granite (WDH-1), yielding a weighted mean $^{206}Pb/^{238}U$ age of 125.8 ± 3.3 Ma, which is consistent with the previously reported Sm—Nd ages (127 ± 4; Jahn et al., 2001). Twenty inherited zircon grains obtained from the Aliwula granite porphyry (ALWY) and granite (ALWG) yield ages varied from 141.9 to 2484.4 Ma (Supplementary Tables 2), which are interpreted as xenocrysts/antecrysts. In addition, two concordant $^{206}Pb/^{238}U$ ages of 124.3 ± 1.0 Ma (1σ, MSWD = 0.48) and 108.8 ± 0.9 (1σ, MSWD = 0.63) Ma, obtained from Aliwula granite porphyry and granite, respectively, are interpreted to represent the emplacement age of the magma.

4.4. Zircon Hf isotopic compositions

Magmatic zircon grains from the studied rocks have positive $\varepsilon_{Hf}(t)$

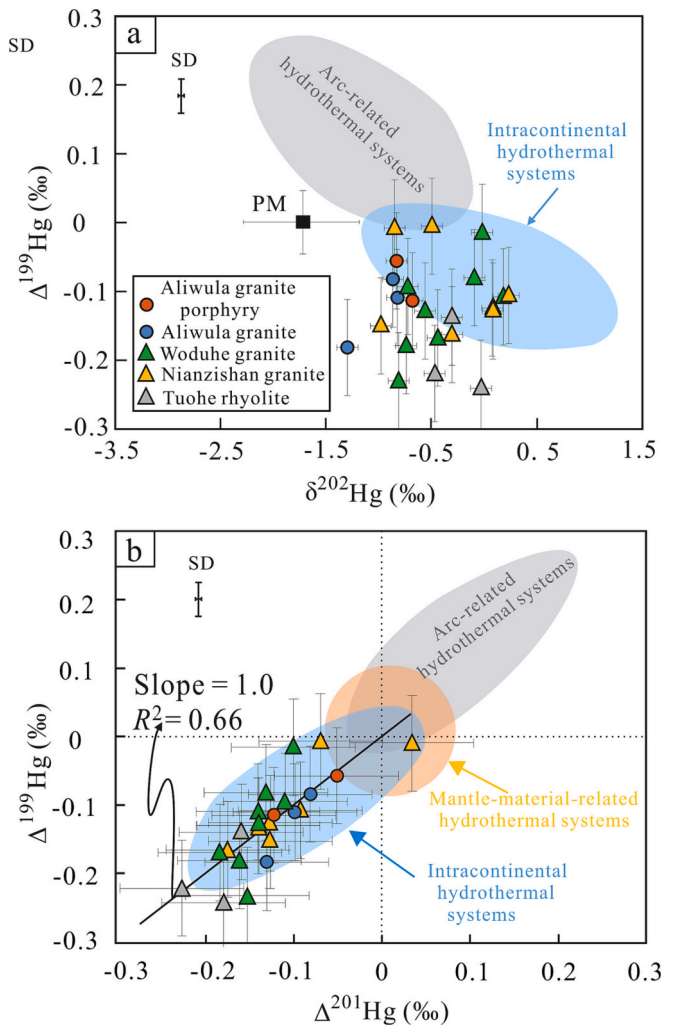

Fig. 6. (a) δ^{202}Hg vs. Δ^{199}Hg and (b) Δ^{201}Hg vs. Δ^{199}Hg plots for the studied granites and rhyolites in NE China. Hg isotopic compositions for arc-related, intracontinental and mantle-related hydrothermal systems refer to Deng et al. (2021, 2022b) and reference therein, and for estimated mantle refer to Meier et al. (2016), and Moynier et al. (2020, 2021).

values of 4.2 to 10.7, falling between the depleted mantle and chondrite evolution lines (Fig. 4b). Xenocryst/antecryst grains from the Aliwula granite porphyry and granite with ages ranging from 141.9 to 1400.9 Ma have low $\varepsilon_{Hf}(t)$ values of −11.5 to 2.9. Zircon grains with low δ^{18}O values generally have high Hf isotopic compositions (Fig. 4c).

4.5. Whole-rock Nd and Hg isotopic compositions

The studied granite and rhyolite samples have $^{147}Sm/^{144}Nd$ and $^{143}Nd/^{144}Nd$ ratios of 0.109889–0.294669 and 0.512668–0.512728, respectively. Based on their zircon U—Pb ages, the initial $^{143}Nd/^{144}Nd$ ratios were calculated to $\varepsilon_{Nd}(t)$ values of −0.5 to 2.4. Nd model ages were calculated by using a two-stage model (Liew and Hofmann, 1988) relative to average continental crust (Jahn and Condie, 1995). The results show that all the Nd two-stage model ages are younger than 1.0 Ga (957–720 Ma; Supplementary Table 4).

The samples have low Hg contents (0.15 to 5.42 ppb), negative to slightly positive δ^{202}Hg values (−1.30 to 0.23‰) and negative Δ^{199}Hg values (−0.24 to −0.01‰) (Fig. 6a). A positive correlation between Δ^{201}Hg and Δ^{199}Hg with $\Delta^{199}Hg/\Delta^{201}Hg$ ratio of 1.0 was observed for these samples (Fig. 6b).

5. Discussion

5.1. Remelting of juvenile upper continental materials

The rhyolite and granite samples in this study are characterized by the enrichment of Nb, Ta and HREEs but the depletion of Sr and Eu (Fig. 3) (Jahn et al., 2001; Wang et al., 2013; Jin, 2018; Qin et al., 2019), which distinguish these rocks from the coeval Nb—Ta depleted arc-like felsic rocks derived from the basaltic lower crust (e.g., Wu et al., 2011; Xu et al., 2013; Deng et al., 2019; Ge et al., 2021) and the adakitic rocks derived from oceanic crust or thickened lower crust in NE China (e.g., Wang et al., 2019; Xu et al., 2020). Compared with the zircons derived from the mantle rocks, the zircon grains with Early Cretaceous ages show mostly lower δ^{18}O values (5.3 ± 0.3‰; Valley et al., 1998), indicating the involvement of meteoric water or sea water during magma genesis (Valley et al., 2005; Boroughs et al., 2012; Smithies et al., 2015). Given the low water solubility in silicic magmas, it is unlikely to generate magmas with low-δ^{18}O (< 5.5‰) via direct magma-water interaction (Boroughs et al., 2012). Therefore, the low-δ^{18}O values of the studied granites and rhyolites indicate that the source rocks had experienced hydrothermal alteration. This finding is consistent with the conclusion of the low-δ^{18}O granites in eastern China (Wei et al., 2002a; Gong et al., 2018). Although the presence of xenocrystic zircon in the Aliwula granite porphyry and granite evidences the assimilation of ancient crustal materials during magma evolution, their high-δ^{18}O values (Fig. 4a) argue against the assimilation of a low-δ^{18}O source.

Previous studies have shown that Hg is relatively rare in silicate matters (Meier et al., 2016). The granites and rhyolite samples in this study have low Hg contents (0.15–5.42 ppb), which is comparable to the previously reported igneous samples (Geng et al., 2018; Moynier et al., 2020). The analytical uncertainties (2SD) of our samples are 0.10‰, 0.06‰ and 0.08‰ for δ^{202}Hg, Δ^{199}Hg, and Δ^{201}Hg, respectively. Therefore, Δ^{199}Hg values lower than −0.06‰ are considered as pronounced Hg-MIF signals. As shown in Fig. 6b, our samples show a $\Delta^{199}Hg/\Delta^{201}Hg$ ratio of 1.0, which is consistent with the ratio observed during aqueous Hg(II) photoreduction (Bergquist and Blum, 2007). Given the occurrence of Hg(II) photoreduction in Earth's surface, the observed negative Δ^{199}Hg values of the granite and rhyolite samples suggest recycling of terrestrial Hg ($\Delta^{199}Hg < 0$; Blum et al., 2014) into deeper reservoirs. The negative Δ^{199}Hg values preclude a source from seawater-altered oceanic crust, considering the positive Δ^{199}Hg values in marine systems (Blum et al., 2014). The felsic rocks develop Hg isotopic compositions that are distinct from those of mantle-derived basalts or ordinary chondrites (Fig. 6a; Meier et al., 2016; Moynier et al., 2020, 2021), but similar to those of intracontinental hydrothermal systems (Fig. 6a; Yin et al., 2019; Deng et al., 2021), indicating the existence of meteoric water-altered magmatic source rocks, or post-solidus hydrothermal overprint. However, the lack of alteration minerals in these samples precludes low-temperature hydrothermal alteration, which is also supported by the zircon O isotopes. The δ^{202}Hg values (−0.47 ± 0.42‰; 1SD, n = 23) in the studied rocks are outside of the compositional fields of the primitive mantle (−1.7‰; Moynier et al., 2021) or crustal materials −0.68 ± 0.45‰; Blum et al., 2014), precluding the significant influence of crustal assimilation. Notably, no linear relationship was observed between Hg and zircon O isotopes, probably due to (1) the large Hg isotopic variation in an individual reservoir (Fig. 6) and (2) the decoupling of Hg and O in zircon due to their different chemical features. Nevertheless, the co-existence of negative Δ^{199}Hg bulk-rock values and low-δ^{18}O zircon values supports that the continental crust was affected by meteoric-water alteration, but excludes marine origin.

The magmatic zircon grains of the rhyolite and granite samples show positive $\varepsilon_{Hf}(t)$ values (Fig. 3b), consistent with the $\varepsilon_{Hf}(t)$ data of late Mesozoic felsic magmatic rocks in NE China, which were regarded as generated by re-melting of juvenile continental crust (Gong et al., 2018; Li et al., 2017; Ge et al., 2021). The felsic rocks in this study have

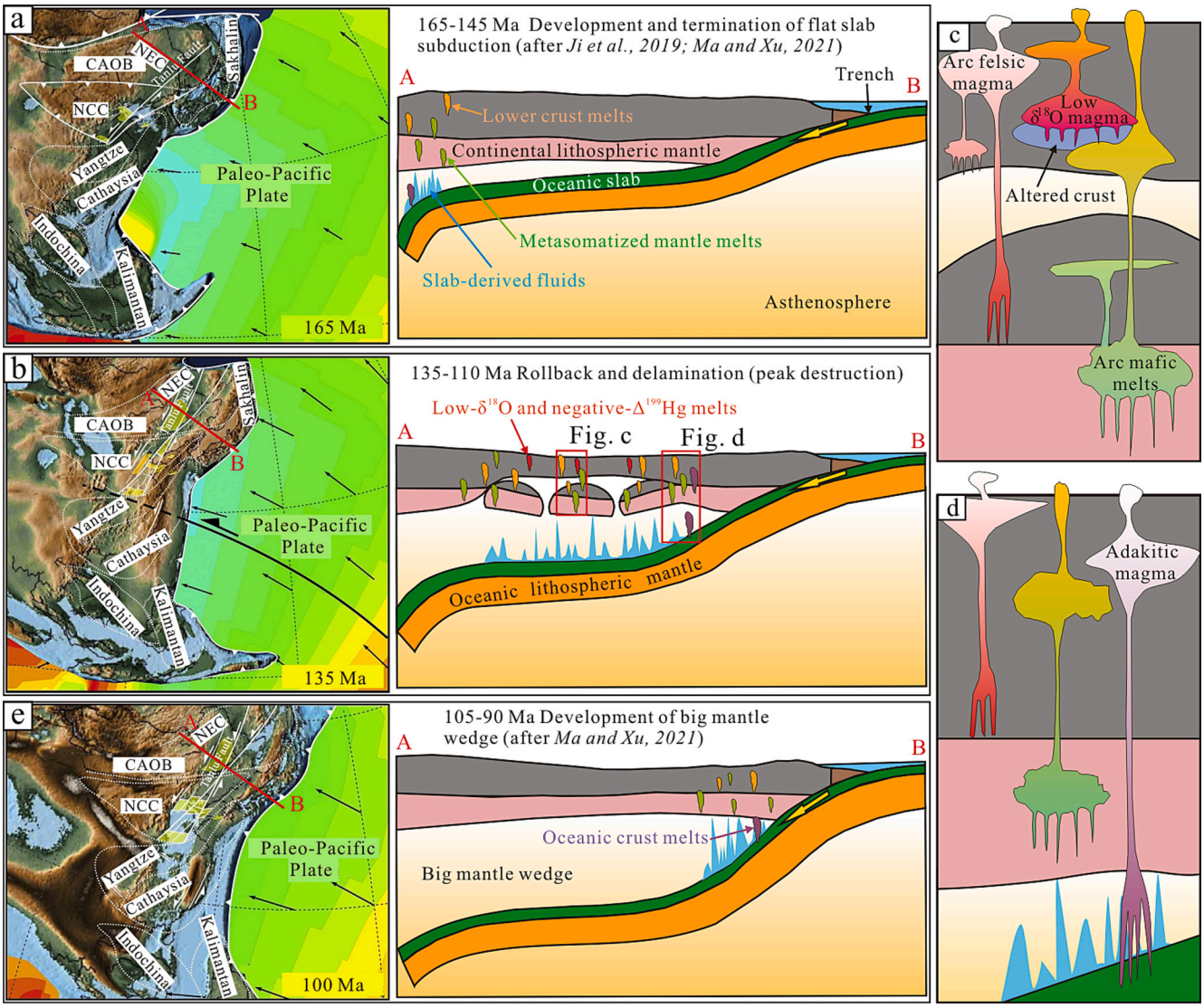

Fig. 7. Cartoons showing the late Mesozoic geodynamic evolution and formation of heterogeneous magmatic rocks in NE China. Paleogeographic and plate reconstructions after Blakey (2016; https://deeptimemaps.com), Müller et al. (2008), and Li et al. (2019). NCC-North China Craton, NEC-NE China, CAOB-Central Asian Orogenic Belt.

Neoproterozoic two-stage model ages (957–720 Ma), indicating a source from the juvenile crust. These juvenile crustal materials were then altered by meteoric water carrying Hg (with negative Δ^{199}Hg values), and were remelted later to produce low-δ^{18}O and negative Δ^{199}Hg melts. Previous studies show that the maximum depth for the effective penetration of water circulation is 5 km (McIntosh and Ferguson, 2021) or ~10 km (Menzies et al., 2014), i.e. within the upper continental crust. Therefore, the low zircon δ^{18}O and positive $\varepsilon_{Hf}(t)$, and negative whole-rock Δ^{199}Hg and slightly positive $\varepsilon_{Nd}(t)$ values indicate hydrothermal alteration and remelting of juvenile rocks within the upper continental crust.

5.2. Orogenic thinning and mantle wedge replenishment

Partial melting of upper crustal rocks in a shallow magma chamber requires high temperature (e.g., Boroughs et al., 2012; Wang et al., 2017). Therefore, the formation of the Early Cretaceous low-δ^{18}O and negative Δ^{199}Hg melts indicates a thermal anomaly to achieve the remelting of the upper juvenile crust in NE China.

Previous studies have suggested that the pre-Jurassic assembly of the NE, North and South China blocks and westward subduction of the Paleo-Pacific oceanic slab since the Jurassic formed the giant ocean-continent subduction zone in East Asia (Fig. 1a; Li et al., 2019 and reference therein). This low-angle subduction of the Paleo-Pacific plate underneath East China during the Jurassic was evidenced by the westward migration of magmatism in NE and North China (Fig. 7a; Ji et al., 2019; Liu et al., 2021; Ma and Xu, 2021; Yang et al., 2021). During the Late Jurassic-Early Cretaceous, the termination of westward migration and subsequent eastward migration of magmatism in NE and North China indicate the rollback or retreat of the Paleo-Pacific oceanic slab (Ji et al., 2019; Ma and Xu, 2021). This mirrors the shift from a compressive to an extensional setting induced by arc retreat (Li et al., 2019 and reference therein). A similar subduction-induced extension is recorded by the development of basins and metamorphic core complexes in eastern China during the Early Cretaceous (Liu et al., 2005; Li et al., 2013; Lin et al., 2013).

Zircon U—Pb ages indicate that the studied low-δ^{18}O and negative Δ^{199}Hg rocks formed in the Early Cretaceous (125.8–108.8 Ma; Fig. 5), coeval with the occurrence of large-scale magmatism in eastern China (Wu et al., 2005; Xu et al., 2013; Deng et al., 2019; Ji et al., 2019) and peak modification of the North China Craton (Zhu et al., 2012; Yang et al., 2021). As a part of the accreted continental margin in East Asia,

lithospheric thinning in NE China occurred simultaneously with the North China Craton modification. Under this kind of extensional setting, Early Cretaceous magmas were formed by the remelting of upper continental crust. The subsequent regional-scale hydrothermal alteration imparted low-$\delta^{18}O$ geochemical features.

Lithospheric delamination in NE China was enabled by regional stress transition from compression to extension, upwelling of asthenosphere and large-volumes of felsic magmatism (e.g., Ducea, 2011; Krystopowicz and Currie, 2013). We propose that crust-mantle interactions during the lithospheric delamination triggered the melting of diverse sources of Early Cretaceous magmatic rocks in NE China. Large-scale release of fluids from the prior-flat slab could have triggered the partial melting of metasomatized mantle and formed the mantle-derived mafic rocks (Fig. 7b; Xu et al., 2013; Deng et al., 2019). Upwelling of the asthenosphere, as compensation of the delaminated lithosphere, would cause the partial melting of the basaltic lower crust and also altered juvenile upper crust, forming granitic rocks with arc-like geochemical features (Wu et al., 2011; Ge et al., 2021) and low-$\delta^{18}O$ felsic rocks (Fig. 7c; Wei et al., 2002a; Gong et al., 2018 and this study). The coeval partial melting of oceanic crust likely produced the adakitic rocks (Fig. 7d; Wang et al., 2019; Xu et al., 2020). $\delta^{18}O$ values of magmatic zircon grains show no correlations with whole-rock geochemistry, Hf, Nd or Hg isotopes, but show a gross correlation with magma ages, with the lowest $\delta^{18}O$ values observed in the igneous rocks of 120–125 Ma (Fig. 4a). This age is coeval with the peak modification of North China Craton (Zhu and Sun, 2021). The lowest $\delta^{18}O$ values probably recorded the strong water-rock interaction occurred at ~125 Ma during the large-scale crustal thinning in NE China (Fig. 7b). Spatially, the younger (< 105 Ma) magmatism in NE China, which mainly occurred adjacent to the subduction zone, was likely caused by the further retreat of the Paleo-Pacific oceanic slab (Fig. 7e; Li et al., 2019; Ma and Xu, 2021).

6. Conclusions and implications

The Early Cretaceous granites and rhyolitesin this study bridges the thermal structure of the orogen in NE China and the tectonic history of eastern China and the Paleo-Pacific plate. The low-$\delta^{18}O$, negative $\Delta^{199}Hg$ and positive zircon $\varepsilon_{Hf}(t)$ and whole-rock $\varepsilon_{Nd}(t)$ values reveal a juvenile upper continental crust origin. Partial melting of upper crustal rocks requires high temperature. The thermal anomaly required for the formation of the low-$\delta^{18}O$ and negative $\Delta^{199}Hg$ magmatic rocks in NE China is contemporaneous with the peak destruction of the North China Craton, which was caused by the roll-back and foundering of the Paleo-Pacific oceanic slab during the Early Cretaceous. This study presents a showcase where Hg isotopes, coupled with O and Nd—Hf isotopes, is a promising tool for petrogenetic studies, although additional work is required.

Supplementary data to this article can be found online at https://doi.org/10.1016/j.chemgeo.2023.121569.

Declaration of Competing Interest

The authors declare that they have no known competing financial interestsor personal relationships that could have appeared to influence the work reported in this paper.

Data availability

Data will be made available on request.

Acknowledgments

We would like to thank Editor Sonja Aulbach, professor Stephen Grasby and anonymous reviewers for the constructive suggestions of the manuscript. This study was supported by the Department of Natural Resources of Heilongjiang Province (201701) and the Croucher Chinese Visitorships from Croucher Foundation (2020−2021). Professor Guosheng Sun is thanked for their help during fieldwork. Professor Min Sun is thanked for the constructive comments on the preparation of the manuscript.

References

Bergquist, B.A., Blum, J.D., 2007. Mass-dependent and -independent fractionation of Hg isotopes by photoreduction in aquatic systems. Science 318, 417–420.
Bindeman, I., Gurenko, A., Carley, T., Miller, C., Martin, E., Sigmarsson, O., 2012. Silicic magma petrogenesis in Iceland by remelting of hydrothermally altered crust based on oxygen isotope diversity and disequilibria between zircon and magma with implications for MORB. Terra Nova 24 (3), 227–232.
Blum, J.D., Bergquist, B.A., 2007. Reporting of variations in the natural isotopic composition of mercury. Anal. Bioanal. Chem. 388, 353–359.
Blum, J.D., Sherman, L.S., Johnson, M.W., 2014. Mercury isotopes in Earth and environmental sciences. Annu. Rev. Earth Planet. Sci. 42, 249–269.
Boroughs, S., Wolff, J.A., Ellis, B.S., Bonnichsen, B., Larson, P.B., 2012. Evaluation of models for the origin of Miocene low-$\delta^{18}O$ rhyolites of the Yellowstone/Columbia River large Igneous Province. Earth Planet. Sci. Lett. 313–314, 45–55.
Cao, H.H., Xu, W.L., Pei, F.P., et al., 2013. Zircon U-Pb geochrology and petrogenesis of the late Pleozoic-early Mesozoic Intrusive rocks in the eastern segment of the northern margin of the North China Block. Lithos 170-171, 191–207.
Chen, D., Ren, D.S., Deng, C.Z., Tian, Z.D., Yin, R.S., 2022. Mercury loss and isotope fractionation during high-pressure and high-temperature processing of sediments: Implication for the behaviors of mercury during metamorphism. Geochim. Cosmochim. Acta 334, 231–240.
Deng, C.Z., Sun, D.Y., Li, G.H., Lu, S., Tang, Z.Y., Gou, J., Yang, Y.J., 2019. Early Cretaceous volcanic rocks in the Great Xing'an Range: late effect of a flat-slab subduction. J. Geodyn. 124, 38–51.
Deng, C.Z., Sun, G.Y., Rong, Y.M., Sun, R.Y., Sun, D.Y., Lehmann, B., Yin, R.S., 2021. Recycling of mercury from the atmosphere-ocean system into volcanic-arc-associated epithermal gold systems. Geology 49, 309–313.
Deng, C.Z., Geng, H.Y., Xiao, T.T., Chen, D., Sun, G.Y., Yin, R.S., 2022a. Mercury isotopic compositions of the Precambrian rocks and implications for tracing mercury cycling in Earth's interior. Precambrian Res. 373, 106646.
Deng, C.Z., Lehmann, B., Xiao, T.T., Tan, Q.P., Chen, D., Tian, Z.D., Wang, X.Y., Sun, G. Y., Yin, R.S., 2022b. Intracontinental and arc-related hydrothermal systems display distinct $\delta^{202}Hg$ and $\Delta^{199}Hg$ features: Implication for large-scale mercury recycling and isotopic fractionation in different tectonic settings. Earth Planet. Sci. Lett. 593, 117646.
Drew, D.L., Bindeman, I.N., Watts, K.E., Schmitt, A.K., Fu, B., Mccurry, M., 2013. Crustal scale recycling in caldera complexes and rift zones along the Yellowstone hotspot track: O and Hf isotopic evidence in diverse zircons from voluminous rhyolites of the Picabo volcanic field, Idaho. Earth Planet. Sci. Lett. 381, 63–77.
Ducea, M.N., 2011. Fingerprinting orogenic delamination. Geology 39, 191–192.
Eiler, J.M., 2001. Oxygen isotope variations of basaltic lavas and upper mantle rocks. Rev. Mineral. Geochem. 43, 319–364.
Eizenhöfer, P.R., Zhao, G.C., 2018. Solonker Suture in East Asia and its bearing on the final closure of the eastern segment of the Palaeo-Asian Ocean. Earth Sci. Rev. 186, 153–172.
Frost, B.R., Barnes, C.G., Collins, W.J., Arculus, R.J., Ellis, D.J., Frost, C.D., 2001. A geochemical classification for granitic rocks. J. Petrol. 42, 2033–2048.
Gao, S., Liu, X.M., Yuan, H.L., Hattendorf, B., Gunther, D., Chen, L., Hu, S.H., 2002. Determination of forty-two major and trace elements in USGS and NIST SRM glasses by laser ablation-inductively coupled plasma-mass spectrometry. Geostand. Newslett. 26, 191–196.
Ge, M.H., Li, L., Wang, T., Zhang, J.J., Tong, Y., Guo, L., Liu, K., Feng, L., Song, P., Yuan, J.G., 2021. Hf isotopic mapping of the Paleozoic-Mesozoic granitoids from the Jiamusi and Songnen blocks, NE China: Implications for their tectonic division and juvenile continental crustal growth. Lithos 386–387, 106048.
Geng, H.Y., Yin, R.S., Li, X.D., 2018. An optimized protocol for high precision measurement of Hg isotopic compositions in samples with low concentrations of Hg using MC-ICP-MS. J. Anal. At. Spectrom. 33, 1932–1940.
Gevedon, M., Lackey, J.S., Barnes, J.D., 2021. Skarn Fluid sources as Indicators of timing of Cordilleran Arc Emergence and Paleogeography in the Southwestern United States. Geology 49, 1317–1321.
Gong, M.Y., Tian, W., Fu, B., Wang, S.Y., Dong, J.L., 2018. Zircon Hf-O isotopic constraints on the origin of late Mesozoic felsic volcanic rocks from the Great Xing'an Range, NE China. Lithos 308-309, 412–427.
Griffin, W.L., Andi, Z., O'Reilly, S.Y., Ryan, C.G., 1998. Phanerozoic Evolution of the Lithosphere beneath the Sino-Korean Craton. In: Flower, M.F.J., Chung, S., Lo, C., Lee, T. (Eds.), Geodynamics Series. American Geophysical Union, Washington, D. C, pp. 107–126.
Huang, Q., Liu, Y., Chen, J., Feng, X., Huang, W., Yuan, S., Cai, H., Fu, X., 2015. An improved dual-stage protocol to pre-concentrate mercury from airborne particles for precise isotopic measurement. J. Anal. At. Spectrom. 30, 957–966.
Jahn, B.M., 2004. The Central Asian Orogenic Belt and growth of the continental crust in the Phanerozoic. Geol. Soc. Lond. Spec. Publ. 226, 73–100.
Jahn, B.M., Condie, K.C., 1995. Evolution of the Kaapvaal Craton as viewed from geochemical and Sm-Nd isotopic analyses of intracratonic pelites. Geochim. Cosmochim. Acta 59, 2239–2258.

Jahn, B., Wu, F.Y., Capdevila, R., Martineau, F., Zhao, Z.H., Wang, Y.X., 2001. Highly evolved juvenile granites with tetrad REE paterns: the Woduhe and Baerzhe granites from the Great Xing'an Mountains in NE China. Lithos 59, 171–198.
Ji, Z., Meng, Q.A., Wan, C.B., Zhu, D.F., Ge, W.C., Zhang, Y.L., Yang, H., Dong, Y., 2019. Geodynamic evolution of flat-slab subduction of Paleo-Pacific palte: Constraints from Jurassic adakitic lavas in the Hailar Basin, NE China. Tectonics 38, 4301–4319.
Jin, R.X., 2018. Mineralogy, petrochemistry, and petrogenesis of Nb-Ta-rich alkaline rhyolite of the Tuohe forest farm in the northern Da Hinggan Mountains. Master Degree Thesis. Jilin University, pp. 1–46 (in Chinese with English abstract).
Kempton, P.D., Harmon, R.S., 1992. Oxygen isotope evidence for large-scale hybridization of the lower crust during magmatic underplating. Geochim. Cosmochim. Acta 56, 971–986.
Krystopowicz, N.J., Currie, C.A., 2013. Crustal eclogitization and lithosphere delamination in orogens. Earth Planet. Sci. Lett. 361, 195–207.
Lackey, J.S., Cecil, M.R., Windham, C.J., Frazer, R.E., Bindeman, I.N., Gehrels, G.E., 2012. The Fine Gold Intrusive Suite: the roles of basement terranes and magma source development in the early cretaceous Sierra Nevada batholith. Geosphere 8, 292–313.
Li, J.H., Zhang, Y.Q., Dong, S.W., Su, J.B., Li, Y., Cui, J.J., Shi, W., 2013. The Hengshan low-angle normal fault zone: Structural and geochronological constraints on the Late Mesozoic crustal extension in South China. Tectonophysics 606, 97–115.
Li, J., Tang, S.H., Zhu, X.K., Pan, C.H., 2016. Production and Certification of the Reference Material GSB 04-3258-2015 as a $^{143}Nd/^{144}Nd$ Isotope Ratio Reference. Geostand. Geoanal. Res. 41, 255–262.
Li, S., Chung, S.L., Wang, T., Wilde, S.A., Chu, M.F., Guo, Q.Q., 2017. Tectonic significance and geodynamic processes of large-scale early cretaceous granitoid magmatic events in the southern Great Xing'an Range, North China. Tectonics 36, 615–633.
Li, S.Z., Suo, Y.H., Li, X.Y., et al., 2019. Mesozoic tectono-magmatic response in the East Asian ocean-continent connection zone to subduction of the Paleo-Pacific plate. Earth Sci. Rev. 192, 91–137.
Liew, T.C., Hofmann, A.W., 1988. Precambrian crustal components, plutonic associations, and plate environment of the Hercynian fold belt of Central Europe: Indications from Nd and Sr isotopic study. Contrib. Mineral. Petrol. 98, 129–138.
Lin, W., Faure, M., Chen, Y., Ji, W., Wang, F., Wu, L., Charles, N., Wang, J., Wang, Q., 2013. Late Mesozoic compressional to extensional tectonics in the Yiwulüshan massif, NE China and its bearing on the evolution of the Yinshan–Yanshan orogenic belt. Part I: Structural analyses and geochronological constraints. Gondwana Res. 23, 54–77.
Liu, J.L., Davis, G.A., Lin, Z.Y., Wu, F.Y., 2005. The Liaonan metamorphic core complex, Southeastern Liaoning Province, North China: a likely contributor to cretaceous rotation of Eastern Liaoning, Korea and contiguous areas. Tectonophysics 407, 65–80.
Liu, Y.S., Gao, S., Hu, Z.C., Gao, C.G., Zong, K.Q., Wang, D.B., 2010. Continental and oceanic crust recycling-induced melt-peridotite interactions in the Trans-North China Orogen: U-Pb dating, Hf isotopes and trace elements in zircons of mantle xenoliths. J. Petrol. 51, 537–571.
Liu, L., Liu, L.J., Xu, Y.G., 2021. Mesozoic intraplate tectonism of East Asia due to flat subduction of a composite terrane slab. Earth Sci. Rev. 214, 103505.
Ludwig, K.R., 2003. ISOPLOT 3.00: A Geochronological Toolkit for Microsoft Excel, vol. 39. Berkeley Geochronology Center, California, Berkeley.
Ma, Q., Xu, Y.G., 2021. Magmatic perspective on subduction of Paleo-Pacific plate and initiation of big mantle wedge in East Asia. Earth Sci. Rev. 213, 103473.
Maniar, P.D., Piccoli, P.M., 1989. Tectonic discrimination of granitoids. Geol. Soc. Am. Bull. 101, 635–643.
McIntosh, J.C., Ferguson, G., 2021. Deep meteoric water circulation in Earth's crust. Geophys. Res. Lett. 48, e2020GL090461.
Meier, M.M.M., Cloquet, C., Marty, B., 2016. Mercury (Hg) in meteorites: Variations in abundance, thermal release profile, mass-dependent and mass-independent isotopic fractionation. Geochim. Cosmochim. Acta 182, 55–72.
Menzies, C.D., Teagle, D.A.H., Craw, D., Cox, S.C., Boyce, A.J., Barrie, C.D., Roberts, S., 2014. Incursion of meteoric waters into the ductile regime in an active orogen. Earth Planet. Sci. Lett. 399, 1–13.
Morel, M.L.A., Nebel, O., Nebel-Jacobsen, Y.J., Miller, J.S., Vroon, P.Z., 2008. Hafnium isotope characterization of the GJ-1 zircon reference material by solution and laser-ablation MC-ICP-MS. Chem. Geol. 255, 231–235.
Moynier, F., Chen, J.B., Zhang, K., Cai, H.M., Wang, Z.C., Jackson, M.G., Day, J.M.D., 2020. Chondritic mercury isotopic composition of Earth and evidence for evaporative equilibrium degassing during the formation of eucrites. Earth Planet. Sci. Lett. 551, 116544.
Moynier, F., Jackson, M.G., Zhang, K., Cai, H., Halldórsson, S.A., Pik, R., et al., 2021. The mercury isotopic composition of Earth's mantle and the use of mass independently fractionated Hg to test for recycled crust. Geophys. Res. Lett. 48, e2021GL094301.
Müller, R.D., Sdrolias, M., Gaina, C., Steinberger, B., Heine, C., 2008. Long-term sea level fluctuations driven by ocean basin dynamics. Science 319, 1357–1362.
Page, F.Z., Fu, B., Kita, N.T., Fournelle, J., Spicuzza, M.J., Schulze, D.J., Viljoen, F., Basei, M.A.S., Valley, J.W., 2007. Zircons from kimberlite: new insights from oxygen isotopes, trace elements, and Ti in zircon thermometry. Geochim. Cosmochim. Acta 71, 3887–3903.
Qin, J.H., Liu, C., Chen, Y.C., Deng, J.F., 2019. Timing of lithospheric extension in northeastern China: evidence from the Late Mesozoic Nianzishan A-type granitoid complex. J. Earth Sci. 30, 689–706.
Rollinson, H., 1993. Using Geochemical Data: Evaluation, Presentation, Interpretation. Willey, New York.
Safonova, I., 2017. Juvenile versus recycled crust in the Central Asian Orogenic Belt: Implications from ocean plate stratigraphy, blueschist belts and intra-oceanic arcs. Gondwana Res. 47, 6–27.
Salters, V.J.M., White, W.M., 1998. Hf isotope constraints on mantle evolution. Chem. Geol. 145, 447–460.
Sláma, J., Kosler, J., Condon, D.J., Crowley, J.L., Gerdes, A., Hanchar, J.M., Horstwood, M.S.A., Morris, G.A., Nasdala, L., Norberg, N., Schaltegger, U., Schoene, B., Tubrett, M.N., Whitehouse, M.J., 2008. Plesovice zircon-A new natural reference material for U-Pb and Hf isotopic microanalysis. Chem. Geol. 249, 1–35.
Smith, C.N., Kesler, S.E., Klaue, B., Blum, J.D., 2005. Mercury isotope fractionation in fossil hydrothermal systems. Geology 33, 825–828.
Smithies, R.H., Kirkland, C.L., Cliff, J.B., Howard, H.M., Quentin de Gromard, R., 2015. Syn-volcanic cannibalisation of juvenile felsic crust: Superimposed giant ^{18}O-depleted rhyolite systems in the hot and thinned crust of Mesoproterozoic Central Australia. Earth Planet. Sci. Lett. 424, 15–25.
Sun, S.S., McDonough, W.F., 1989. Chemical and isotopic systematic of oceanic basalts: Implication for mantle composition and processes. In: Sunders, A.D., Norry, M.J. (Eds.), Magmatic in Oceanic Basins, 42. Geological Society of London Special Publication, pp. 313–345.
Tian, Z.D., Leng, C.B., Deng, C.Z., Zhang, X.C., Chen, D., Gao, L.J., Wang, X.Y., Yin, R.S., 2022. Mercury isotopes as a useful tracer of magma source: an example from the Daocheng-Cuojiaoma batholith, eastern Tibetan Plateau. Chem. Geol. 605, 120974.
Valley, J.W., Chiarenzelli, J.R., McLelland, J.M., 1994. Oxygen isotope geochemistry of zircon. Earth Planet. Sci. Lett. 126, 187–206.
Valley, J.W., Kinny, P.D., Schulze, D.J., Spicuzza, M.J., 1998. Zircon megacrysts from kimberlite: Oxygen isotope variability among mantle melts. Contrib. Mineral. Petrol. 133, 1–11.
Valley, J.W., Lackey, J.S., Cavosie, A.J., Clechenko, C.C., Spicuzza, M.J., Basei, M.A.S., Bindeman, I.N., Ferreira, V.P., Sial, A.N., King, E.M., Peck, W.H., Sinha, A.K., Wei, C. S., 2005. 4.4 billion years of crustal maturation: oxygen isotope ratios of magmatic zircon. Contrib. Mineral. Petrol. 150, 561–580.
Wang, J.G., He, Z.H., Xu, W.L., 2013. Petrogenesis of riebeckite rhyolites in the southern Da Hinggan Mts.: Geochronological and geochemical evidence. Acta Petrol. Sin. 29, 853–863.
Wang, Z.J., Xu, W.L., Pei, F.P., et al., 2015. Geochronology and geochemistry of Middle Permian-Middle Triassic Intrusive rocks from Central-Eastern Jilin Province, NE China: Constraints on the tectonic evolution of the eastern segment of the Paleo-Asian Ocean. Lithos 238, 13–25.
Wang, W., Cawood, P.A., Zhou, M.-F., Pandit, M.K., Xia, X.-P., Pandit, M.K., Xia, X.-P., Zhao, J.-H., 2017. Low-$\delta^{18}O$ rhyolites from the Malani igneous suite: a positive test for South China and NW India linkage in Rodinia. Geophys. Res. Lett. 40, 10298–10305.
Wang, F., Xu, W.L., Xing, K.C., Tang, J., Wang, Z.W., Sun, C.Y., Wu, W., 2019. Temporal changes in the subduction of the Paleo-Pacific plate beneath Eurasia during the late Mesozoic: Geochronological and geochemical evidence from cretaceous volcanic rocks in eastern NE China. Lithos 326-327, 415–434.
Wang, X.Y., Deng, C.Z., Yang, Z.Y., Zhu, J.J., Yin, R.S., 2021. Oceanic mercury recycled into the mantle: evidence from positive $\Delta^{199}Hg$ in lamprophyres. Chem. Geol. 584, 120505.
Wei, C.S., Zheng, Y.F., Zhao, Z.F., Valley, J.W., 2002a. Oxygen and neodymium isotope evidence for recycling of juvenile crust in Northeast China. Geology 30, 375–378.
Wei, G.J., Liang, X.R., Li, X.H., Liu, Y., 2002b. Precise measurement of Sr isotopic composition of liquid and solid base using (LP) MC-ICPMS. Geochimica 31, 295–299.
Wei, C.S., Zhao, Z.F., Spicuzza, M.J., 2008. Zircon oxygen isotopic constraint on the sources of late Mesozoic A-type granites in eastern China. Chem. Geol. 250, 1–15.
Whalen, J.B., Currie, K.L., Chappell, B.W., 1987. A-type granites: geochemical characteristics, discrimination and petrogenesis. Contrib. Mineral. Petrol. 95, 407–419.
Windley, B.F., Xiao, W.J., 2018. Ridge subduction and slab windows in the Central Asian Orogenic Belt: Tectonic Implications for the evolution of an accretionary orogen. Gondwana Res. 61, 73–87.
Wu, F.Y., Lin, J.Q., Wilde, S.A., Zhang, X.O., Yang, J.H., 2005. Nature and significance of the Early Cretaceous giant igneous event in Eastern China. Earth Planet. Sci. Lett. 233, 103–119.
Wu, F.Y., Yang, Y.H., Xie, L.W., Yang, J.H., Xu, P., 2006. Hf isotopic compositions of the standard zircons and baddeleyites used in U-Pb geochronology. Chem. Geol. 234, 105–126.
Wu, F.Y., Sun, D.Y., Ge, W.C., Zhang, Y.B., Grant, M.L., Wilde, S.A., Jahn, B.M., 2011. Geochronology of the Phanerozoic granitoids in northeastern China. J. Asian Earth Sci. 41, 1–30.
Wu, F.Y., Yang, J.H., Xu, Y.G., Wilde, S.A., Walker, R.J., 2019. Destruction of the North China Craton in the Mesozoic. Annu. Rev. Earth Planet. Sci. 47, 173–195.
Xiao, W.J., Windley, B.F., Sun, S., Li, J.L., Huang, B.C., Han, C.M., Yuan, C., Sun, M., Chen, H.L., 2015. A tale of amalgamation of three Permo-Triassic collage systems in Central Asia: oroclines, sutures, and terminal accretion. Annu. Rev. Earth Planet. Sci. 43, 477–507.
Xu, W.L., Pei, F.P., Wang, F., Meng, E., Ji, W.Q., Yang, D.B., Wei, W., 2013. Spatial-temporal relationships of Mesozoic volcanic rocks in NE China: Constraints on tectonic overprinting and transformations between multiple tectonic regimes. J. Asian Earth Sci. 74, 167–193.
Xu, G.Z., Deng, C.Z., Li, C.L., Lv, C.L., Yin, R.S., Ding, J.S., Yuan, M.W., Gou, J., 2020. Petrogenesis of Late Carboniferous A-type granites and Early Cretaceous adakites of the Songnen Block, NE China: Implications for the geodynamic evolution of the Paleo-Asian and Paleo-Pacific oceans. Lithos 366–367, 105575.

Yang, W.B., Niu, H.C., Sun, W.D., Shan, Q., Zheng, Y.F., Li, N.B., Li, C.Y., Arndt, N.T., Xu, X., Jiang, Y.H., Yu, X.Y., 2013. Isotopic evidence for continental ice sheet in mid-latitude region in the super greenhouse early cretaceous. Sci. Rep. 3, 2732.
Yang, Y.T., Guo, Z.X., Song, C.C., Li, X.B., He, S., 2015. A short-lived but significant Mongol-Okhotsk collisional orogeny in latest Jurassic-earliest cretaceous. Gondwana Res. 28, 1096–1116.
Yang, J.H., Xu, L., Sun, J.F., Zeng, Q., Zhao, Y.N., Wang, H., Zhu, Y.S., 2021. Geodynamics of decratonization and related magmatism and mineralization in the North China Craton. Sci. China Earth Sci. 64 (9), 1409–1427.
Yin, R.S., Krabbenhoft, D.P., Bergquist, B.A., Zheng, W., Lepak, R.F., Hurley, J.P., 2016. Effects of mercury and thallium concentrations on high precision determination of mercury isotopic composition by Neptune Plus multiple collector inductively coupled plasma mass spectrometry. J. Anal. At. Spectrom. 31, 2060–2068.
Yin, R.S., Deng, C.Z., Lehmann, B., Sun, G.Y., Lepak, R.F., Hurley, J.P., Zhao, C.H., Xu, G. W., Tan, Q.P., Xie, G.Z., Hu, R.Z., 2019. Magmatic-hydrothermal origin of mercury in Carlin-style and epithermal gold deposits in China: evidence from mercury stable isotopes. ACS Earth Space Chem. 3, 1631–1639.
Yin, R.S., Chen, D., Pan, X., Deng, C.Z., Chen, L.M., Song, X.Y., Yu, S.Y., Zhu, C.W., Wei, X., Xu, Y., Feng, X.B., Blum, J.D., Lehmann, B., 2022. Mantle Hg isotopic heterogeneity and evidence of oceanic Hg recycling into the mantle. Nat. Commun. 13, 948.
Zerkle, A.L., Yin, R.S., Chen, C.Y., Li, X.D., Izon, G.J., Grasby, S.E., 2020. Anomalous fractionation of mercury isotopes in the late Archean atmosphere. Nat. Commun. 11, 1709.
Zhao, G.C., Wang, Y.J., Huang, B.C., Dong, Y.P., Li, S.Z., Zhang, G.W., Yu, S., 2018. Geological reconstructions of the East Asian blocks: from the breakup of Rodinia to the assembly of Pangea. Earth Sci. Rev. 186, 262–286.
Zheng, Y.F., 1993. Calculation of oxygen isotope fractionation in anhydroussilicate minerals. Geochim. Cosmochim. Acta 57, 1079–1091.
Zheng, Y.F., Mao, J.W., Chen, Y.J., Sun, W.D., Ni, P., Yang, X.Y., 2019. Hydrothermal ore deposits in collisional orogens. Sci. Bull. 64, 205–212.
Zhu, R.X., Sun, W.D., 2021. The big mantle wedge and decratonic gold deposits. Sci. China Earth Sci. 64 (9), 1451–1462.
Zhu, R.X., Xu, Y.G., 2019. The subduction of the West Pacific plate and the destruction of the North China Craton. Sci. China Earth Sci. 62, 1340–1350.
Zhu, R.X., Yang, J.H., Wu, F.Y., 2012. Timing of destruction of the North China Craton. Lithos 149, 51–60.